Electronic Supplementary Material (ESI) for Journal of Materials Chemistry A.

Supporting Information

Construction of Triple Heterogeneous Interfaces Optimizing Electronic Structure with B-doped Amorphous CoP Deposited on Crystalline Cu_2S/Ni_3S_2 Nanosheets to Enhance Water Electrolysis

Yajuan Zhang[a,b], Hui Xu[a*], Xingwei Shi[b*], Yuanhai Bao[a], Yong Chen[a]

[a] *Key Laboratory of Low Carbon Energy and Chemical Engineering of Gansu Province, College of Petrochemical Technology, Lanzhou University of Technology, Lanzhou, 730050, China.*

[b] *Beijing Key Laboratory of Ionic Liquids Clean Process, Center of Ionic Liquids and Low Carbon Energy, Institute of Process Engineering, Chinses Academy of Sciences, Beijing, 100190, China.*

* Corresponding authors.

E-mail addresses: xuhui@lut.edu.cn (H. Xu); xwshi@ipe.ac.cn (X. Shi).

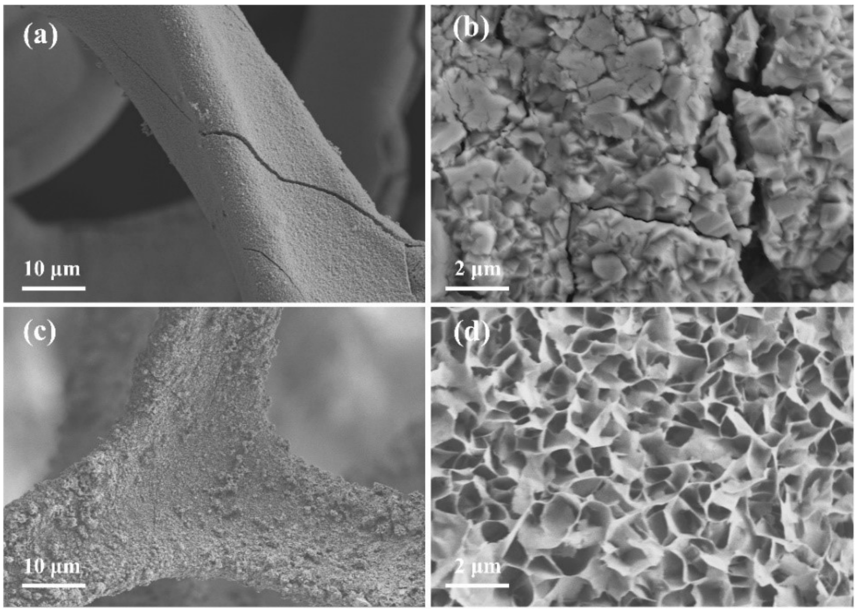

Figure S1. The SEM images of (a, b) Ni_3S_2 and (c, d) Cu_2S/Ni_3S_2 on the nickel foam substrate.

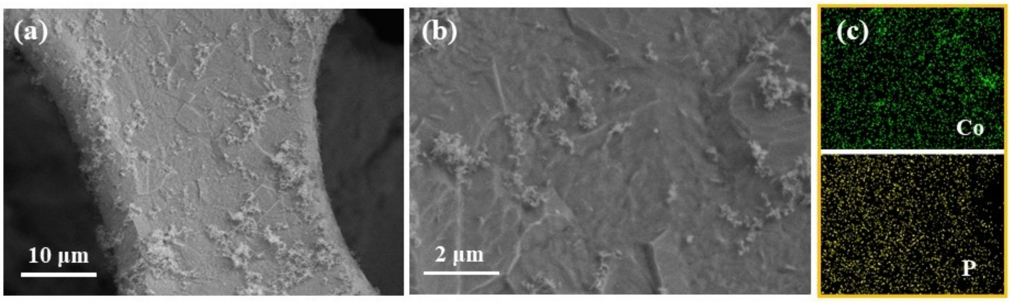

Figure S2. The SEM images of (a, b) CoP on the nickel foam substrate by electroless plating technique and (c) corresponding elemental mapping of Co and P.

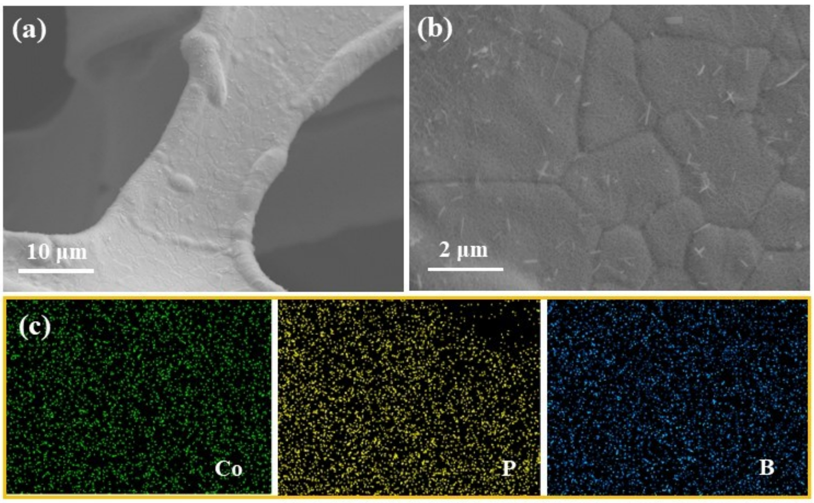

Figure S3. The SEM images of (a, b) CoPB on the nickel foam substrate by electroless plating technique and (c) corresponding elemental mapping of Co, P and B.

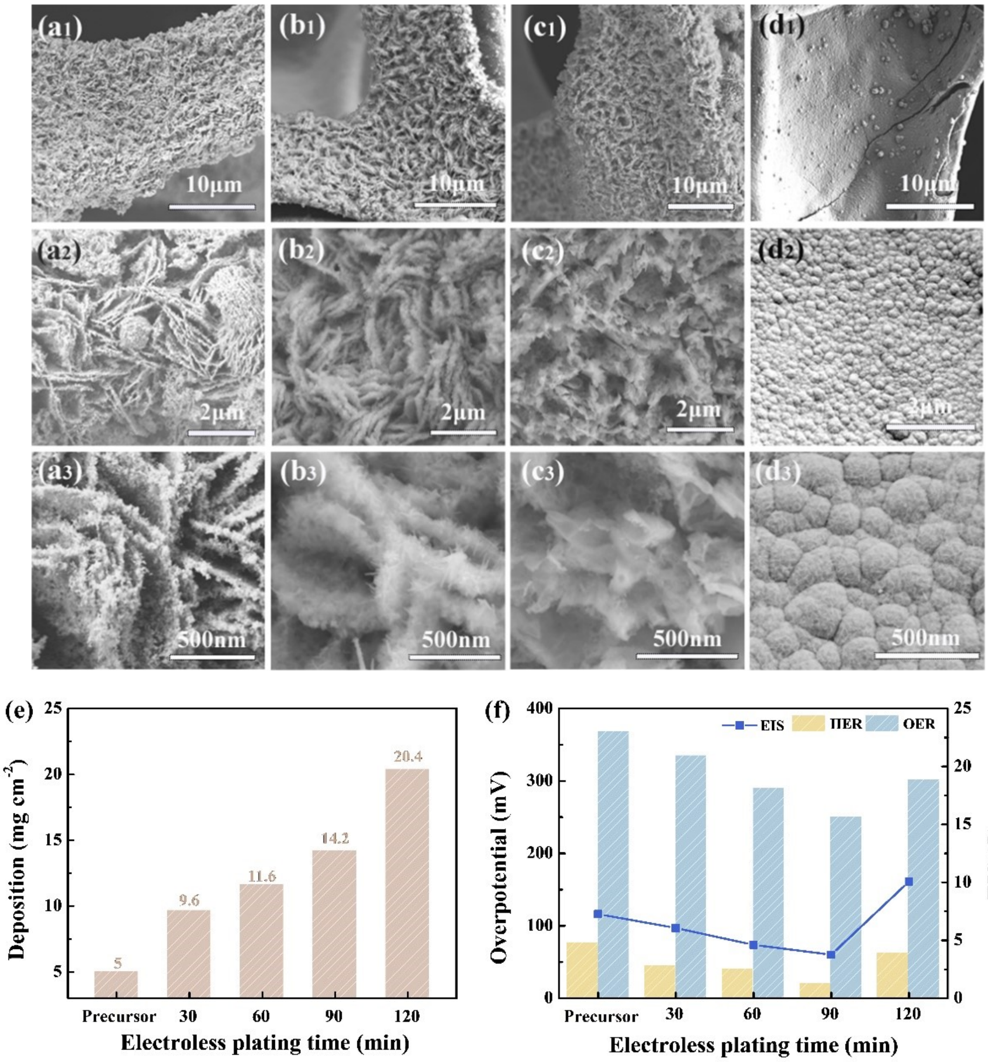

Figure S4. The SEM images of CoPB@Cu_2S/Ni_3S_2 at different plating times (a_1–a_3) 30 min, (b_1–b_3) 60 min, (c_1–c_3) 90min and (d_1–d_3) 120 min. (e) Deposition amount of CoPB@Cu_2S/Ni_3S_2 at different time interval. (f) The overpotential of HER and OER for the CoPB@Cu_2S/Ni_3S_2 on the nickel foam substrate as well as the EIS values represented by the line plot.

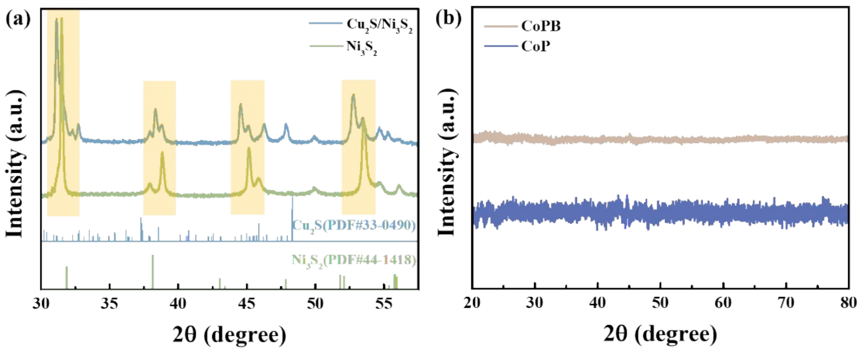

Figure S5. XRD patterns and enlarged XRD patterns of (a) Ni_3S_2, Cu_2S/Ni_3S_2 and (b) CoP, CoPB samples.

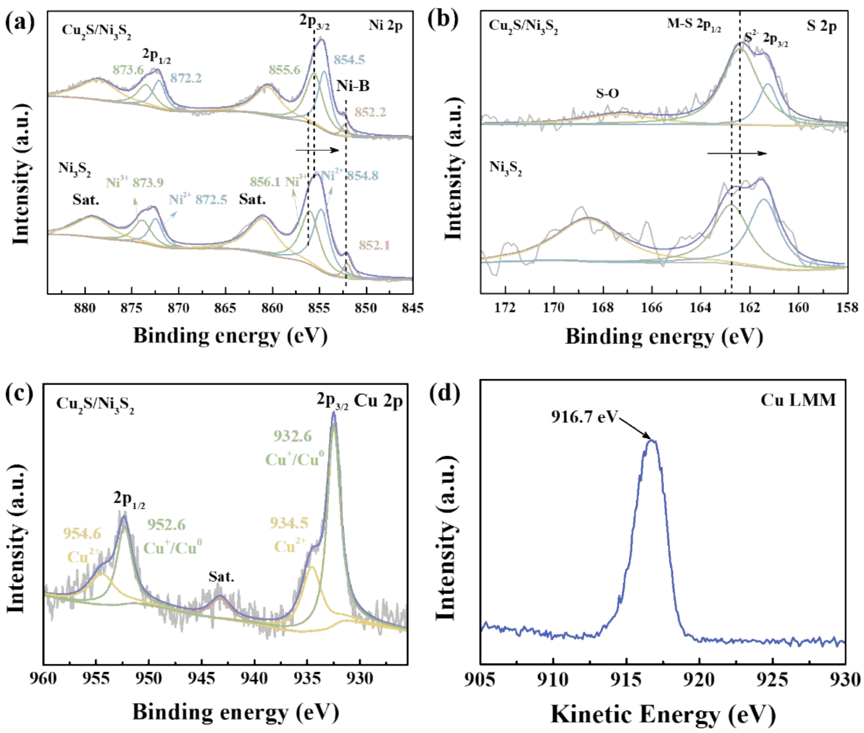

Figure S6. The high-resolution XPS spectra of Ni_3S_2 and Cu_2S/Ni_3S_2 (a) Ni 2p, (b) S 2p, (c) Cu 2p and (d) Cu Auger XPS spectra.

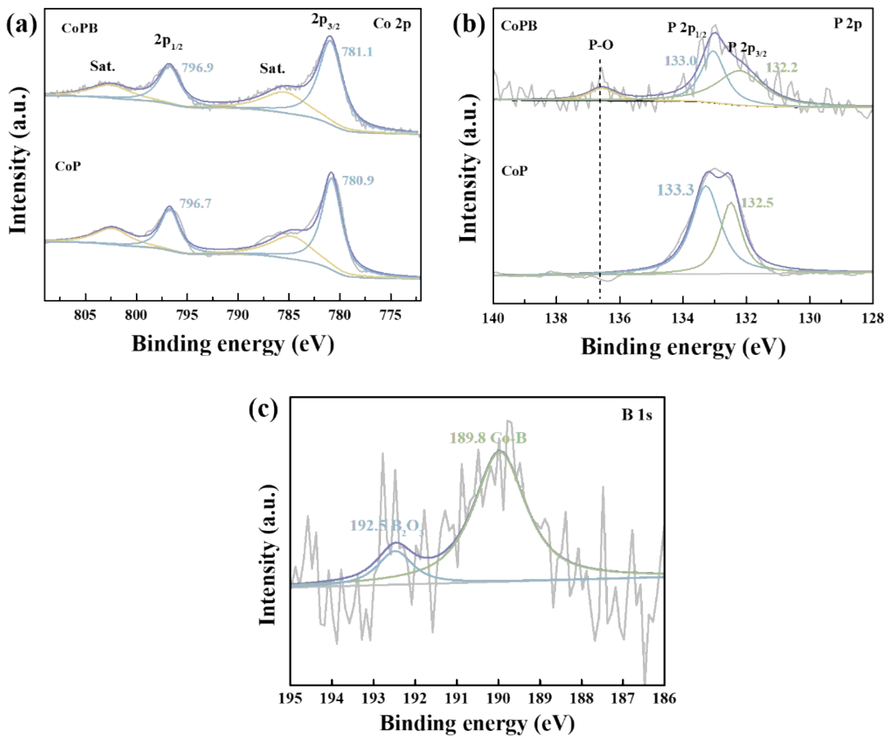

Figure S7. The high-resolution XPS spectra of CoP and CoPB (a) Co 2p, (b) P 2p and (c) B 1s.

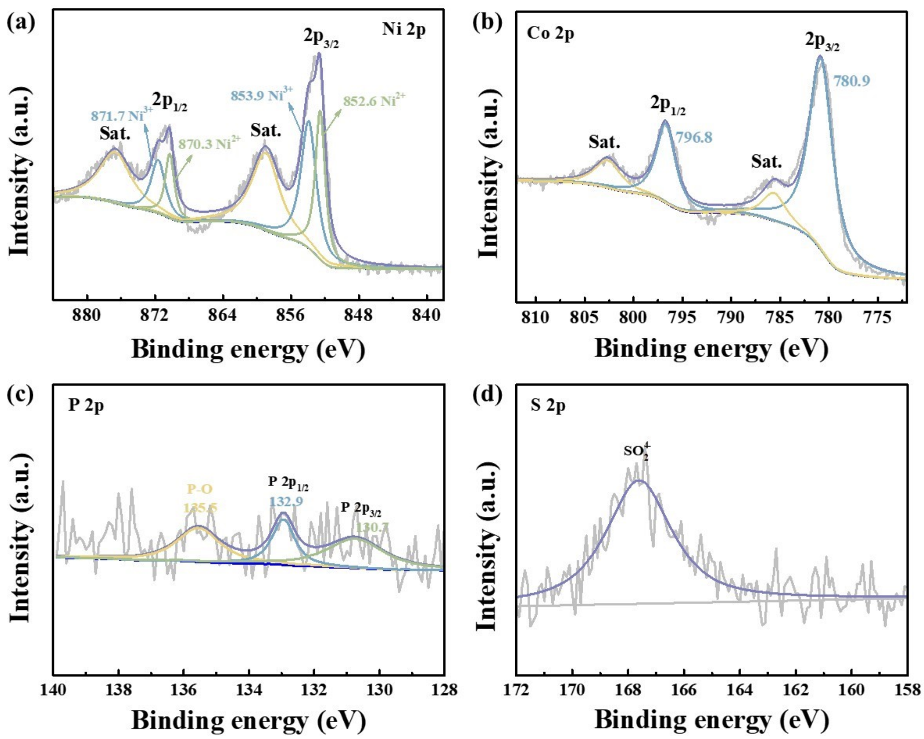

Figure S8. The high-resolution XPS spectra of CoP@Ni_3S_2 (a) Ni 2p, (b) Co 2p, (c) P 2P and (d) S 2P.

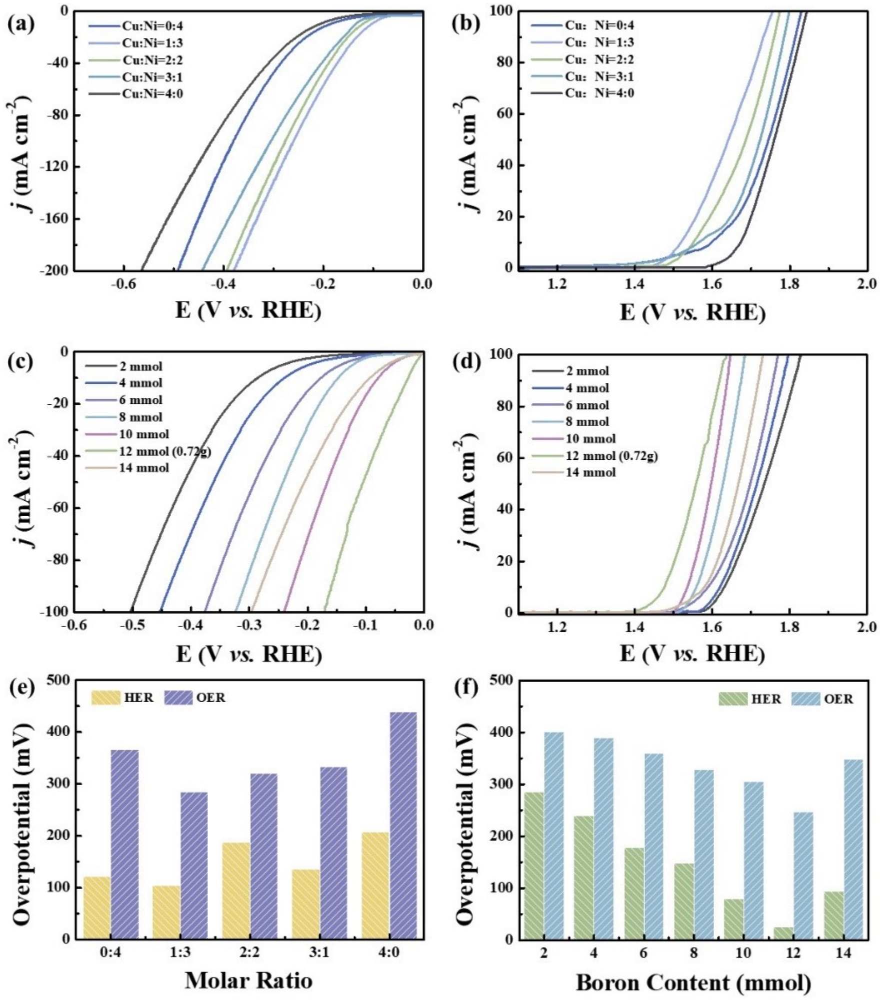

Figure S9. The effect of (a, b, e) different metal ratio (Cu: Ni) in precursor Cu_2S/Ni_3S_2 and (c, d, f) boron content on CoPB layer on HER and OER performance of CoPB@Cu_2S/Ni_3S_2.

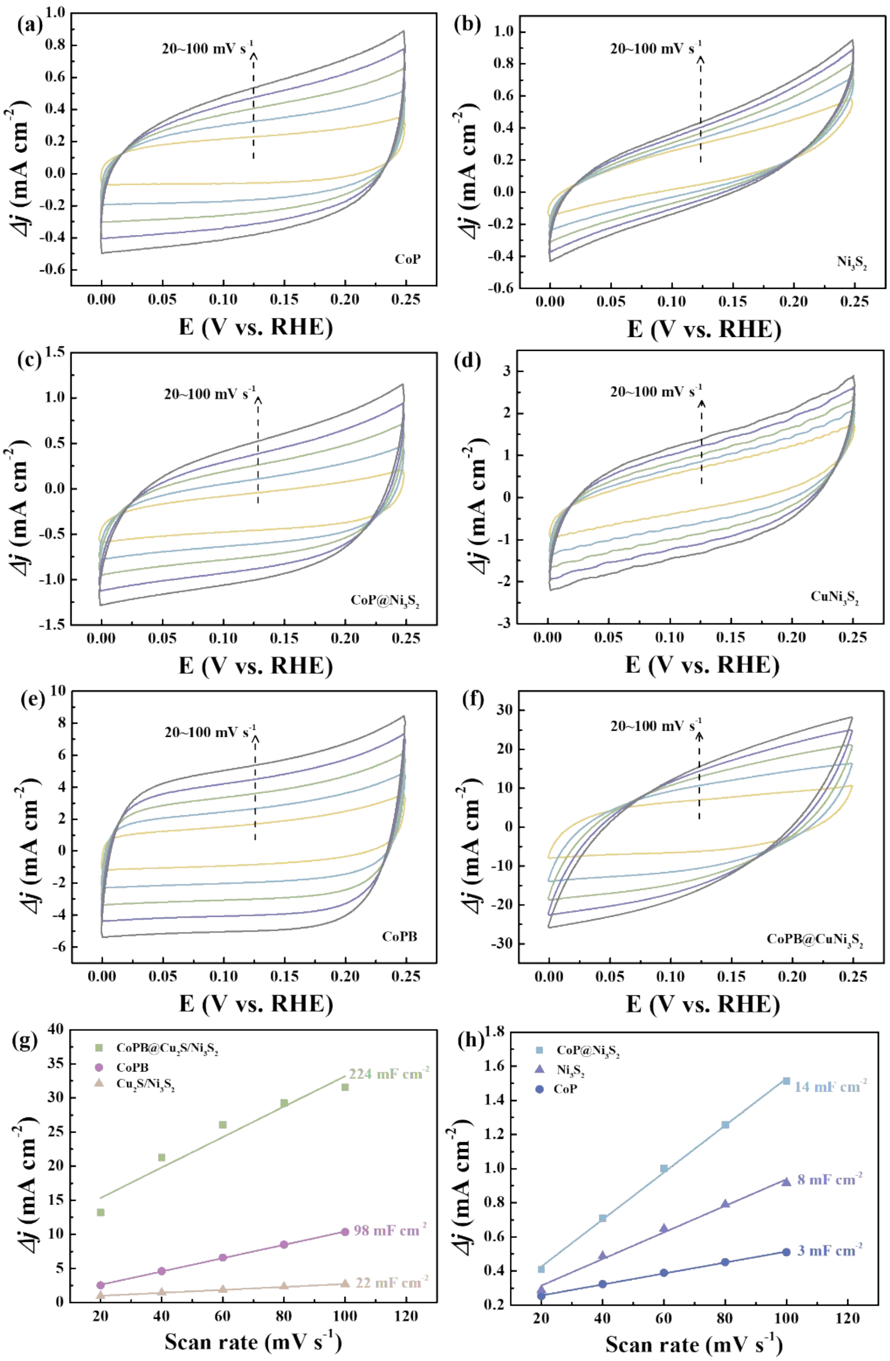

Figure S10. Cyclic voltammograms (CV) curves in the non-Faradaiccurrent range at scan rates of 20, 40, 60, 80 and 100 mV s^{-1} for HER. (a) CoP, (b) Ni_3S_2, (c) CoP@Ni_3S_2, (d) Cu_2S/Ni_3S_2, (e) CoPB, (f) CoPB@Cu_2S/Ni_3S_2. (e, f) The corresponding plots of current density as a function of scan rates.

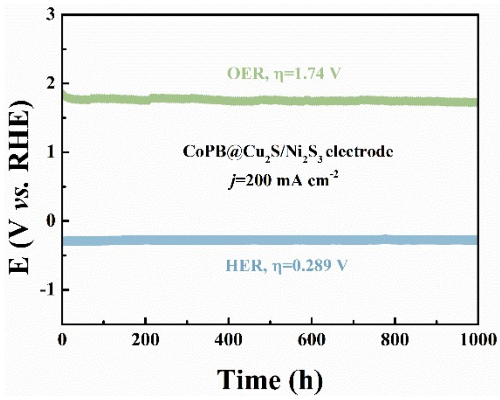

Figure S11. Chronopotentiometry test of long-term stability of CoPB@Cu_2S/Ni_3S_2 electrodes at the current density of 200 mA cm^{-2} for 1000 h.

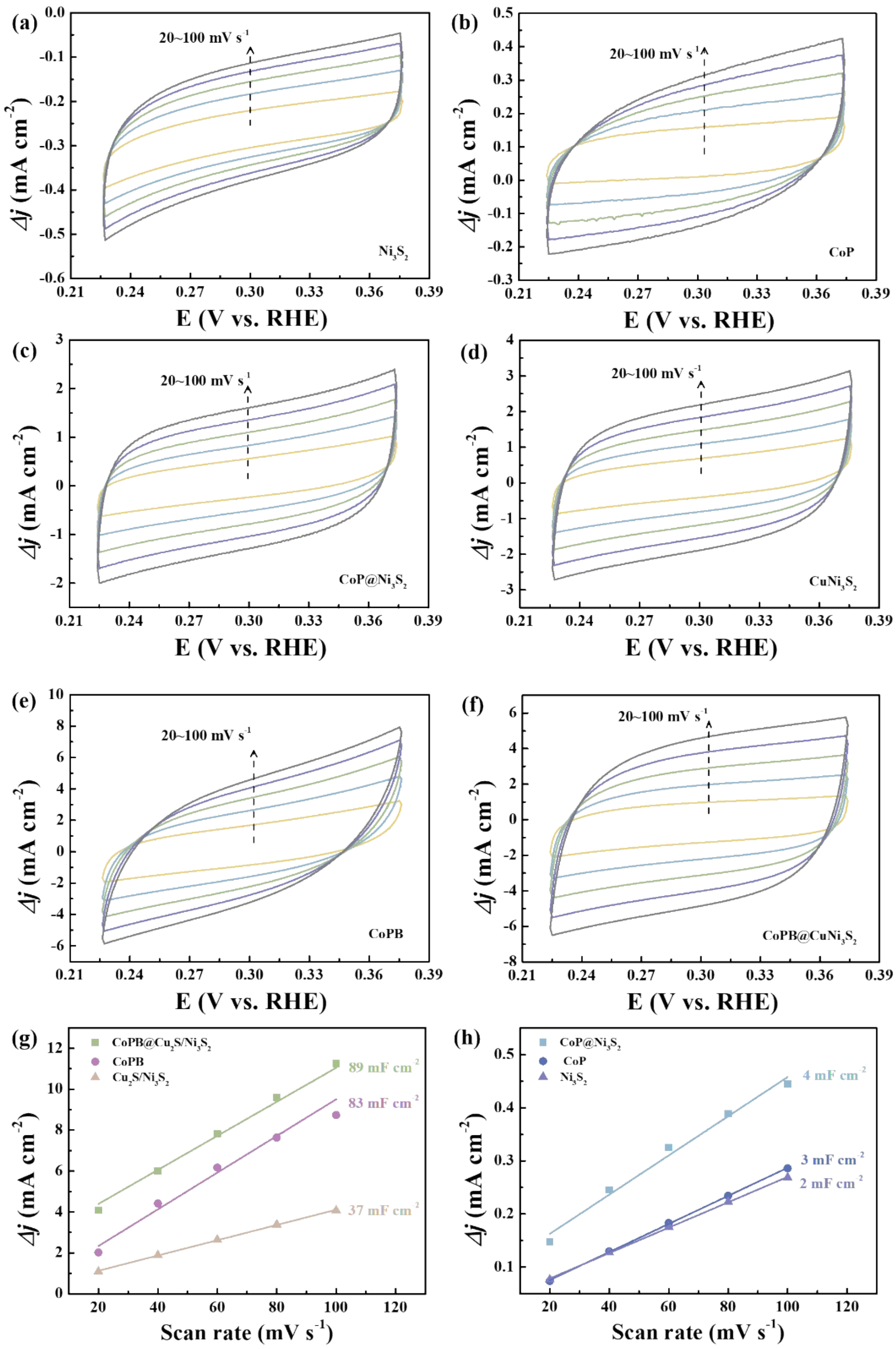

Figure S12. Cyclic voltammograms (CV) curves in the non-Faradaiccurrent range at scan rates of 20, 40, 60, 80 and 100 mV s^{-1} for OER. (a) CoP, (b) Ni_3S_2, (c) CoP@Ni_3S_2, (d) Cu_2S/Ni_3S_2, (e) CoPB, (f) CoPB@Cu_2S/Ni_3S_2. (e, f) The corresponding plots of current density as a function of scan rates.

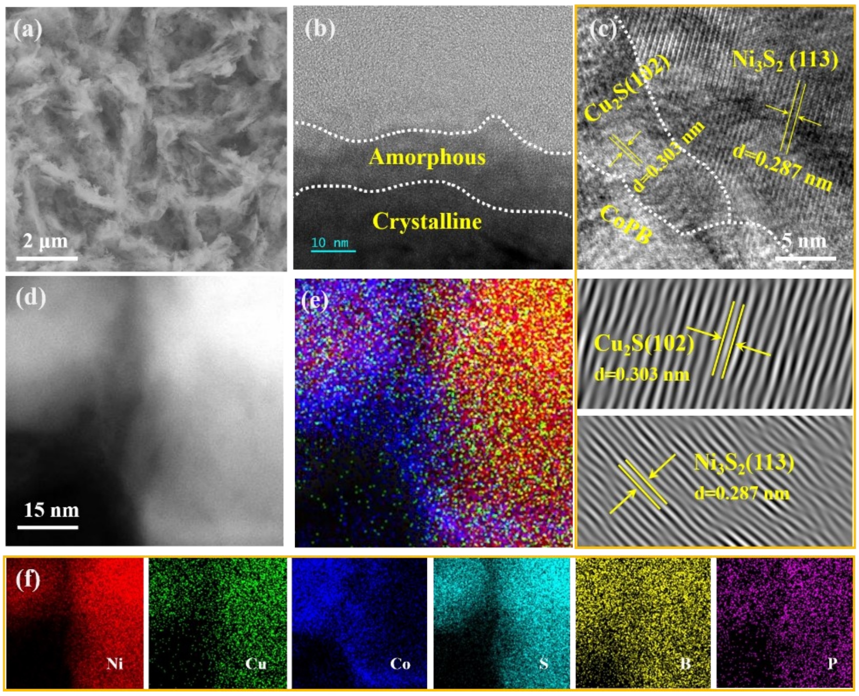

Figure S13. The morphology and internal structure of CoPB@Cu_2S/Ni_3S_2 electrode after HER stability tests at 10 mA cm^{-2}. (a) SEM, (b) TEM, (c) HR-TEM, (d) HADDF-STEM, (e) overlay image and (h) EDX elemental mapping.

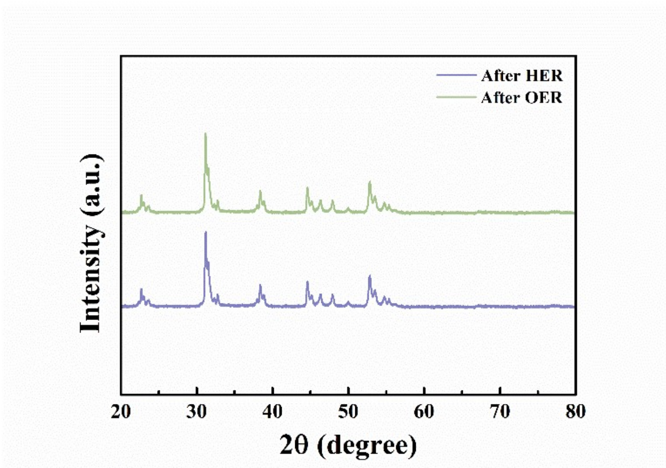

Figure S14. The XRD of HER and OER CoPB@Cu_2S/Ni_3S_2 electrode after operation at 10 mA cm^{-2} for 100 h.

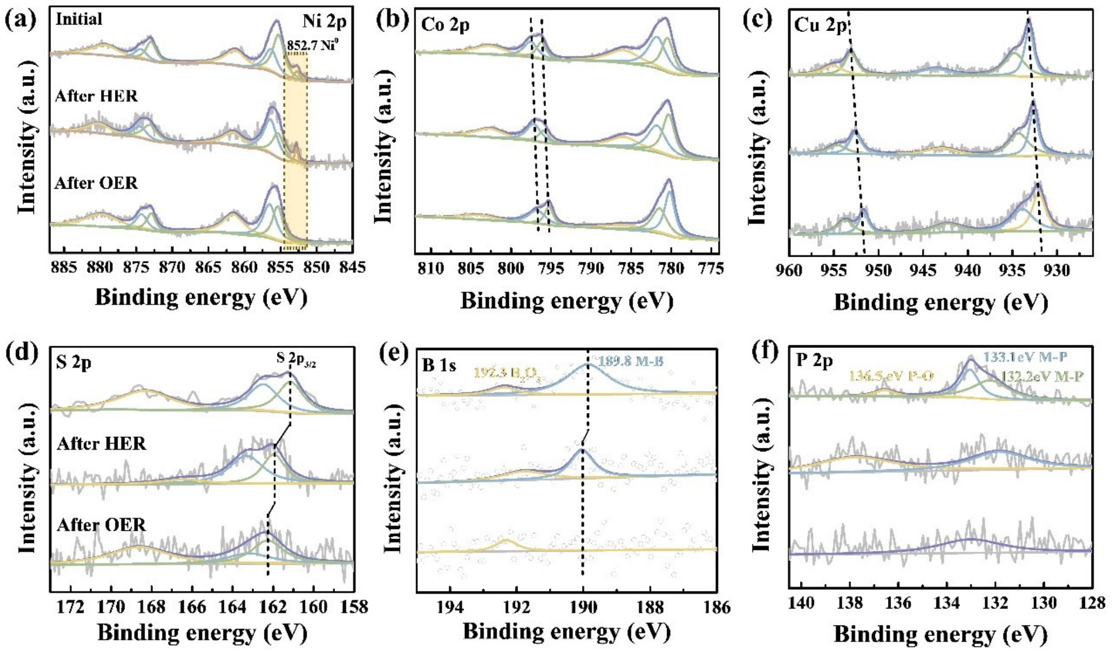

Figure S15. High-resolution XPS spectra of (a) Ni 2p, (b) Co 2p, (c) Cu 2p, (d) S 2p, (e) B 1s and (f) P 2p for the CoPB@Cu_2S/Ni_3S_2 electrode before and after HER and OER stability tests at 10 mA cm^{-2}.

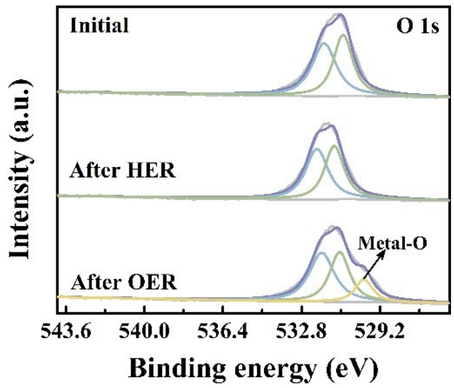

Figure S16. High-resolution XPS spectra of O 1s for the CoPB@Cu_2S/Ni_3S_2 electrode before and after HER and OER stability tests at 10 mA cm^{-2}.

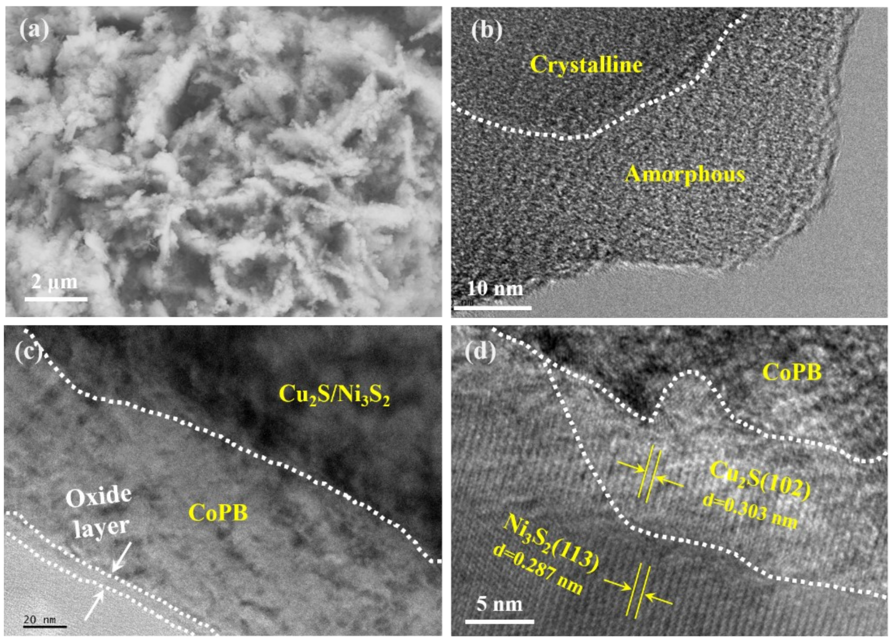

Figure S17. The morphology and internal structure of CoPB@Cu_2S/Ni_3S_2 electrode after OER stability tests at 10 mA cm^{-2}. (a) SEM, (b) TEM and (c, d) HR-TEM images.

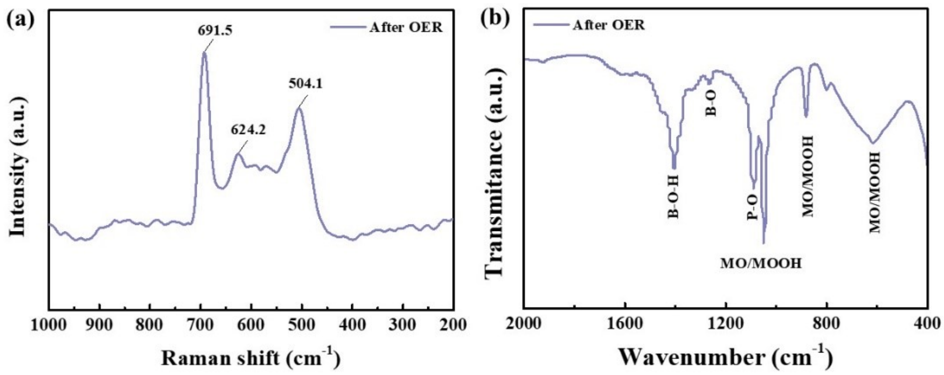

Figure S18. (a) Raman and (b) FTIR spectra of $CoPB@Cu_2S/Ni_3S_2$ after OER test.

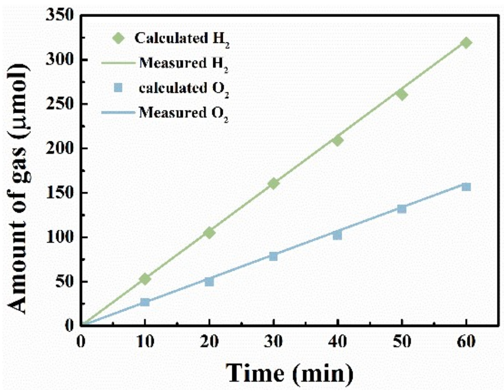

Figure S19. Amount of gas theoretically calculated and experimentally measured versus time for $CoPB@Cu_2S/Ni_3S_2 \| CoPB@Cu_2S/Ni_3S_2$.

Table S1 The resistance (R_s) of $CoPB@Cu_2S/Ni_3S_2$ sample at different deposition.

Catalyst	R_s ($\Omega \cdot sq^{-1}$)			
	30min	60min	90min	120min
$CoPB@Cu_2S/Ni_3S_2$	1.451	1.406	1.195	1.654

Table S2 ICP-AES analysis of electrocatalysts under different deposition times.

Catalyst	wt%					
	Cu	Ni	S	Co	P	B
Cu_2S/Ni_3S_2	16.1	71.4	12.3	-	-	-
CoPB	-	-	-	92.3	5.4	2.231
$CoPB@Cu_2S/Ni_3S_2$-30min	5.5	84.7	3.7	5.3	0.3	0.265
$CoPB@Cu_2S/Ni_3S_2$-60min	8.2	79.5	3.1	8.0	0.4	0.345
$CoPB@Cu_2S/Ni_3S_2$-90min	11.6	73.9	3.8	9.5	0.6	0.410
$CoPB@Cu_2S/Ni_3S_2$-120min	12.0	69.0	4.6	12.3	0.9	0.541

Table S3 EXAFS data fitting results of $CoPB@Cu_2S/Ni_3S_2$.

Sample	Path	CN^a	R(Å)^b	σ^2 (Å^2)^c	ΔE_0(eV)^d	R factor
sample-Co	Co-P/B	4.4	2.25	1.4	-10.4	0.09
	Co-Co/Cu	6.4	2.43	14	-10.4	
sample-Cu	Cu-S	3.3	2.25	0.6	2.2	0.3
	Cu-Ni/Co	6.3	2.61	2.9	2.2	
sample-Ni	Ni-S	4.2	2.26	0.0125	-11.8	0.0111
	Ni-Ni/Cu	6.9	2.50	0.0124	-5.3	

^{a}*CN*, coordination number; ^{b}*R*, the distance between absorber and backscatter atoms; $^c\sigma^2$, the Debye Waller factor value; $^d\Delta E_0$, inner potential correction to account for the difference in the inner potential between the sample and the reference compound; *R* factor indicates the goodness of the fit. $S0^2$ was fixed to 0.804, according to the experimental EXAFS fit of Ni foil by fixing *CN* as the known crystallographic value. * This value was fixed during EXAFS fitting, based on the known structure of Ni. Fitting conditions: *k* range：3.0-12.5; *R* range: 1.0-3.0; fitting space: R space; *k*-weight = 3. A reasonable range of EXAFS fitting parameters: $0.800 < S_0^2 < 1.000$; $CN > 0$; $\sigma^2 > 0$ Å^2; $|\Delta E_0| < 15$ eV; *R* factor < 0.02.

Table S4 comparisons of $CoPB@Cu_2S/Ni_3S_2$ and other electrocatalysts for electrochemical water splitting in 1.0 M KOH.

Catalysts	substrate	*j* (mA cm^{-2})	η(mV) HER	η(mV) OER	Voltages (V)	Reference
$CoPB@Cu_2S/Ni_3S_2$	**NF**	**10**	**25**	**247**	**1.44**	**This work**
$Co_2Mo_1S_x$	NF	10	146	276	1.52	1
CNS/LDH/NF	NF	10	161	230	1.63	2
$SnFeS_xO_y$/NF	NF	10	85	-	-	3
CoS_x/Ni_3S_2@NF	NF	10	204	280	1.57	4
Bi_2S_3/Ni_3S_2/NF	NF	10	-	268	-	5
H-Fe-CoMoS	NF	10	137	282	1.60	6
Ag_2S-NiS_x	NF	10	230	260	1.68	7
$Ni_3(BO_3)_2-Ni_3S_2$/NF	NF	10	92	217	1.49	8
NiS_2/MoS_2-2	NF	10	90	270	-	9
LMOS-4	NF	10	109	300	1.50	10
$Mo-NiS/Ni_3S_2-S_v$	NF	10	73	-	-	11
Co_xP@Ni-Co-S/NF	NF	50	-	271	-	12
$Ni_3S_2/NiCo_2S_4$/NF	NF	100	-	330	-	13
CoMoP/CoP/NF	NF	100	127	308	-	14
Ni_2P@CoP	CC	10	55	-	-	15
$CoMoNiP/Cu_3P$-5	CF	100	106	243	1.65	16
$NiFeP_X@NiCo_2P_X$	NF	10	97	230	1.56	17
CoP-FeP	CC	10	71	250	-	18
Fe_2P/Ni_2P	NF	10	64	185	1.49	19
Mn-CoP/NiPO	CC	10	116	245	-	20
$Cu-NiP_x/NiSe_y$	NF	10	69	-	-	21
$Co@CoP_2$	CF	10	55	210	1.54	22
NiCo/NiCoP	NF	10	-	290	-	23
$NiCoP/NiCoS_x$	NF	10	68	-	-	24
V-CNS/P/NF	NF	10	38	210	1.56	25
$F-NiP_x/Ni_3S_2$-NF	NF	100	182	370	1.55	26
$Mo-NiP_x/NiS_y$	NF	10	85	137	1.42	27
$Co_{0.68}Fe_{0.32}P$	-	10	116	240	-	28
NiFeSP/NF	NF	10	91	-	-	29

Table S5 HER intrinsic activity (TOF) parameters for developing each electrocatalysts was investigated in 1 M KOH.

Catalyst	**C_{dl} (mF cm^{-2})**	**ESCA (cm^2)**	**Turnover frequency TOF (s^{-1})**
$CoPB@Cu_2S/Ni_3S_2$	224	3733.3	1.32
CoPB	98	1633.3	0.96
Cu_2S/Ni_3S_2	22	366.7	0.92
$CoP@Ni_3S_2$	14	233.3	0.81
Ni_3S_2	8	133.3	0.25
CoP	3	50	0.15

Table S6 EIS parameters were calculated of HER and OER electrodes via fitting equivalent circuit.

Catalysts		R_s (Ω)	R_{ct} (Ω)
$CoPB@Cu_2S/Ni_3S_2$	HER	1.10	1.07
	OER	1.36	2.31
CoPB	HER	1.14	2.92
	OER	1.48	3.23
Cu_2S/Ni_3S_2	HER	1.11	6.21
	OER	1.47	3.43
$CoP@Ni_3S_2$	HER	1.06	8.35
	OER	1.51	4.48
Ni_3S_2	HER	1.32	8.61
	OER	1.57	4.32
CoP	HER	1.11	8.41
	OER	1.53	6.89

Table S7 OER intrinsic activity (TOF) parameters for developing each electrocatalysts was investigated in 1 M KOH.

Catalyst	**C_{dl} (mF cm^{-2})**	**ESCA (cm^2)**	**Turnover frequency TOF (s^{-1})**
$CoPB@Cu_2S/Ni_3S_2$	89	1483.3	0.210
CoPB	83	1383.3	0.151
Cu_2S/Ni_3S_2	37	616.7	0.115
$CoP@Ni_3S_2$	4	66.7	0.057
CoP	3	50	0.054
Ni_3S_2	2	33.3	0.039

Table S8 A summary of AEM cell performance in 1M KOH based on published research.

Catalysts	**j (mA cm^{-2})**	**Voltages (V)**	**Reference**
$CoPB@Cu_2S/Ni_3S_2$||$CoPB@Cu_2S/Ni_3S_2$	**1000/2000**	**1.8/1.9**	**This work**
CM||CMOH-5x	1000	2.2	ACS Appl. Mater. Interfaces 2023, **15**, 9231-9239
NiCoOx:Fe||NiCoOx:Fe	1000	2.4	ACS Catalysis, 2019, **9**, 7-15
$CoSb_2O_6$||$CoSb_2O_6$	800	1.9	ACS Energy Lett. 2021, **6**, 364-370
M-Mo-CoP/(CF)||NiFe-LDH/(IF)	1000	1.8	Electrochim. Acta 2023, **472**, 143429
NiFe_FA_NN||NiFeP_FA_NN	500	2.14	Appl. Catal. B: Environ. 2023, **322**, 122101
Mo-NiS||Mo-NiS	1000	2.0	Adv. Funct. Mater. 2023, **33**, 2210656
CuNi@NiSe||CuNi@NiSe	1000	2.2	Small 2023, **19**, 2301613
IrO_2||$RuSe_2$	730	1.8	Small 2021, **17**, 2007333
Ru-Ru_2P/V_2CTx||RuO_2	1000/2000	1.80/2.05	Appl. Catal. B: Environ. 2024, **343**, 123517

References

(1) Shit, S.; Chhetri, S.; Bolar, S.; Murmu, N. C.; Jang, W.; Koo, H.; Kuila, T. Hierarchical Cobalt Sulfide/Molybdenum Sulfide Heterostructure as Bifunctional Electrocatalyst towards Overall Water Splitting. *ChemElectroChem* **2019**, *6*, 430-438.

(2) Zhang, W.; Wang, S.; Wang, Z.; Cao, G.; Zhang, P.; Liu, C. Constructing the heterostructure of sulfide and layered double hydroxide as bifunctional electrocatalyst for overall water splitting. *J. Solid State Electrochem.* **2022**, *27*, 575-583.

(3) Zhang, T.; Han, J.; Tang, T.; Sun, J.; Guan, J. Binder-free bifunctional SnFe sulfide/oxyhydroxide heterostructure electrocatalysts for overall water splitting. *Int. J. Hydrogen Energy* **2023**, *48*, 4594-4602.

(4) Shit, S.; Chhetri, S.; Jang, W.; Murmu, N. C.; Koo, H.; Samanta, P.; Kuila, T. Cobalt Sulfide/Nickel Sulfide Heterostructure Directly Grown on Nickel Foam: An Efficient and Durable Electrocatalyst for Overall Water Splitting Application. *ACS Appl. Mater. Interfaces* **2018**, *10* (33), 27712-27722.

(5) Wang, S.; Xue, W.; Fang, Y.; Li, Y.; Yan, L.; Wang, W.; Zhao, R. Bismuth activated succulent-like binary metal sulfide heterostructure as a binder-free electrocatalyst for enhanced oxygen evolution reaction. *J. Colloid Interface Sci.* **2020**, *573*, 150-157.

(6) Guo, Y.; Zhou, X.; Tang, J.; Tanaka, S.; Kaneti, Y. V.; Na, J.; Jiang, B.; Yamauchi, Y.; Bando, Y.; Sugahara, Y. Multiscale structural optimization: Highly efficient hollow iron-doped metal sulfide heterostructures as bifunctional electrocatalysts for water splitting. *Nano Energy* **2020**, *75*, 104913.

(7) Zhang, H.; Tang, H.; Weng, Q.; Wei, Q.; Duan, M.; Bo, X.; Fu, F.; Zan, L. Engineering heterostructure of bimetallic nickel-silver sulfide as an efficient electrocatalyst for overall water splitting in alkaline media. *J. Solid State Chem.* **2022**, *316*, 123556.

(8) Sun, Z.; Wang, X.; Yuan, M.; Yang, H.; Su, Y.; Shi, K.; Nan, C.; Li, H.; Sun, G.; Zhu, J.; et al. "Lewis Base-Hungry" Amorphous-Crystalline Nickel Borate-Nickel Sulfide Heterostructures by In Situ Structural Engineering as Effective Bifunctional Electrocatalysts toward Overall Water Splitting. *ACS Appl. Mater. Interfaces* **2020**, *12*, 23896-23903.

(9) Qian, Y.; Yu, J.; Zhang, Y.; Zhang, F.; Kang, Y.; Su, C.; Shi, H.; Kang, D. J.; Pang, H.

Interfacial Microenvironment Modulation Enhancing Catalytic Kinetics of Binary Metal Sulfides Heterostructures for Advanced Water Splitting Electrocatalysts. *Small Methods* **2022**, *6*, e2101186.

(10) Shit, S.; Bolar, S.; Murmu, N. C.; Kuila, T. Minimal lanthanum-doping triggered enhancement in bifunctional water splitting activity of molybdenum oxide/sulfide heterostructure through structural evolution. *Chem. Eng. J.* **2022**, *428*, 131131.

(11) Zhang, K.; Duan, Y.; Graham, N.; Yu, W. Unveiling the synergy of polymorph heterointerface and sulfur vacancy in NiS/Ni_3S_2 electrocatalyst to promote alkaline hydrogen evolution reaction. *Appl. Catal. B: Environ.* **2023**, *323*, 122144.

(12) Li, M.; Zheng, K.; Zhang, J.; Li, X.; Xu, C. Design and construction of 2D/2D sheet-on-sheet transition metal sulfide/phosphide heterostructure for efficient oxygen evolution reaction. *Appl. Surf. Sci.* **2021**, *565*, 150510

(13) Wang, J.; Guo, Z.; Yu, Y.; Yu, H.; Yang, J.; Luo, Y.; Xue, Y.; Cai, N.; Li, H.; Yu, F. Polysulfide-Induced Synthesis of Hierarchical $Ni_3S_2/NiCo_2S_4$ Nanorods Supported on Nickel Foam for Boosted Oxygen Evolution Catalysis. *J. Phys. Chem. C* **2023**, *127*, 4808-4815.

(14) Wei, Y.; Li, W.; Li, D.; Yi, L.; Hu, W. Amorphous-crystalline cobalt-molybdenum bimetallic phosphide heterostructured nanosheets as Janus electrocatalyst for efficient water splitting. *Int. J. Hydrogen Energy* **2022**, *47*, 7783-7792.

(15) Tang, W.; Wang, J.; Guo, L.; Teng, X.; Meyer, T. J.; Chen, Z. Heterostructured Arrays of $Ni_xP/S/Se$ Nanosheets on $Co_xP/S/Se$ Nanowires for Efficient Hydrogen Evolution. *ACS Appl. Mater. Interfaces* **2017**, *9*, 41347-41353.

(16) Jin, J.; Chen, F.; Feng, Y.; Zhou, J.; Lei, W.; Gao, F. Co-Ni-Mo phosphides hierarchical nanoarrays as bifunctional electrocatalysts for excellent overall water splitting. *Fuel* **2023**, *332*, 126131.

(17) Wang, Z.; Heng, N.; Wang, X.; He, J.; Zhao, Y. Surface and morphology structure evolution of metal phosphide for designing overall water splitting electrocatalyst. *J. Catal.* **2019**, *374*, 51-59.

(18) Niu, Z.; Qiu, C.; Jiang, J.; Ai, L. Hierarchical CoP–FeP Branched Heterostructures for Highly Efficient Electrocatalytic Water Splitting. *ACS Sustainable Chem. Eng.* **2018**, *7* (2), 2335-2342.

(19) Wang, X.; Wang, B.; Chen, Y.; Wang, M.; Wu, Q.; Srinivas, K.; Yu, B.; Zhang, X.; Ma, F.; Zhang, W. Fe_2P nanoparticles embedded on Ni_2P nanosheets as highly efficient and stable

bifunctional electrocatalysts for water splitting. *J. Mater. Scie. Technol.* **2022**, *105*, 266-273.

(20) Liu, Y.; Gong, W.; Yao, S.; Liang, Y.; Yang, Y.; Yu, T.; Yuan, C.; Yang, Y. Synergistically Coupling of Manganese-Doped CoP Nanowires Arrays with Highly Dispersed $Ni(PO_3)_2$ Nanoclusters toward Efficient Overall Water Splitting. *Inorg. Chem.* **2022**, *61*, 14201-14210.

(21) Han, B.; Du, X.; Li, J.; Wang, H.; Liu, G.; Li, J. Synergistic effect of Cu doping and NiPx/NiSey heterostructure construction for boosted water electrolysis. *Appl. Surf. Sci.* **2022**, *604*, 154617.

(22) Sun, Y.; Liu, T.; Li, Z.; Meng, A.; Li, G.; Wang, L.; Li, S. Morphology and interfacial charge regulation strategies constructing 3D flower-like Co@CoP_2 heterostructure electrocatalyst for efficient overall water splitting. *Chem. Eng. J.* **2022**, *433*, 133684.

(23) Shao, Z.; Qi, H.; Wang, X.; Sun, J.; Guo, N.; Huang, K.; Wang, Q. Boosting oxygen evolution by surface nitrogen doping and oxygen vacancies in hierarchical NiCo/NiCoP hybrid nanocomposite. *Electrochim. Acta* **2019**, *296*, 259-267.

(24) Han, W.; Zhang, F.; Qiu, L.; Qian, Y.; Hao, S.; Li, P.; He, Y.; Zhang, X. Interface engineering of hierarchical NiCoP/$NiCoS_x$ heterostructure arrays for efficient alkaline hydrogen evolution at large current density. *Nanoscale* **2022**, *14*, 15498-15506.

(25) Suo, N.; Dou, Z.; Cui, L. Interface and composition engineering of vanadium doped cobalt nickel sulfide/phosphide heterostructure for efficient water splitting. *Electrochim. Acta* **2021**, *368*, 137602.

(26) Li, K.; Tong, Y.; Feng, D.; Chen, P. Fluorine-anion engineering endows superior bifunctional activity of nickel sulfide/phosphide heterostructure for overall water splitting. *J. Colloid Interface Sci.* **2022**, *625*, 576-584.

(27) Wang, J.; Zhang, M.; Yang, G.; Song, W.; Zhong, W.; Wang, X.; Wang, M.; Sun, T.; Tang, Y. Heterogeneous Bimetallic Mo-NiP_x/NiS_y as a Highly Efficient Electrocatalyst for Robust Overall Water Splitting. *Adv. Funct. Mater.* **2021**, *31*, 2101532.

(28) Li, F.; Bu, Y.; Lv, Z.; Mahmood, J.; Han, G. F.; Ahmad, I.; Kim, G.; Zhong, Q.; Baek, J. B. Porous Cobalt Phosphide Polyhedrons with Iron Doping as an Efficient Bifunctional Electrocatalyst. *Small* **2017**, *13*, 1701167.

(29) Xin, Y.; Kan, X.; Gan, L. Y.; Zhang, Z. Heterogeneous Bimetallic Phosphide/Sulfide Nanocomposite for Efficient Solar-Energy-Driven Overall Water Splitting. *ACS Nano* **2017**, *11*,

10303-10312.